CHAPTER 4

THE PROPOSED LTC WITH COPPER LOSS MINIMIZATION

4.1 Introduction

In the previous chapter, the extension of the operation range to the field weakening range by using the proposed LTC such that the IPMSM drive can operate over much wider speed range had been presented. In this chapter, in order to further minimize the copper loss during the steady state operation as well as to achieve fast transient response, the proposed linear torque control (LTC) strategy is also extended to the entire field weakening region to achieve full range maximum torque per ampere control. In fact, due to its linearity characteristic, this linear control strategy is especially convenient for the synchronous control of multiple IPMSM drives. It is found that in the partial field weakening region, the existing maximum torque per ampere control happens to be the same as the proposed LTC under lighter load condition. In other words, the proposed control can achieve the objective of minimum copper loss (i.e. maximum torque per ampere) for the entire speed range. Sound theoretical basis is given in the context. Moreover, an adaptive limiter is proposed for efficiently implementing the proposed control strategy over the entire speed range. Finally, a prototype is also constructed by using a fixed point DSP TMS320F240 and some experimental results are given to verify the validity of the proposed control strategy.

4.2 The Proposed Linear Maximum Torque Per Ampere (LMTPA) Control—Constant Torque Limit Region

For convenience, the steady state d- and q-axis equivalent circuits of an IPMSM in the

rotor reference frame are given in Fig. 4.1. The corresponding d- and q-axis voltage equations of Fig. 4.1 had been given in (2.6) and (2.7). The corresponding generated electromagnetic torque was also given in (2.5). Also for a practical inverter-fed motor drive, there exists an inverter output voltage limit and an output current limit. Assume that the maximum available phase voltage magnitude and the maximum line current magnitude are V_{sm} and I_{sm} respectively. Then the feasible operation range is constrained by the current limit inequality of (2.21) and the voltage limit inequality of (2.22).

From (2.5) one can observe that when i_{ds} is equal to zero, then the resulting T_e is proportional to i_{qs}. Hence, it is quite simple to implement a high performance drive as in [8-10]. However, the reluctance torque of the IPMSM is not fully exploited. In case i_{ds} is not equal to zero, then it is seen that T_e contains a nonlinear term, namely $0.75\,p\,(L_d\text{-}L_q)\,i_{ds}\,i_{qs}$ rendering the controller design much more difficult than a linear one.

As far as achieving fast transient response is concerned, the maximum torque per ampere control [12-16] is rather attractive. For a given torque demand, the line current magnitude, or $\sqrt{i_{ds}^2+i_{qs}^2}$ equivalently, is minimized to achieve the maximum torque per ampere ratio. Within the current constraint of (2.21), the d- and q-axis stator currents should satisfy the

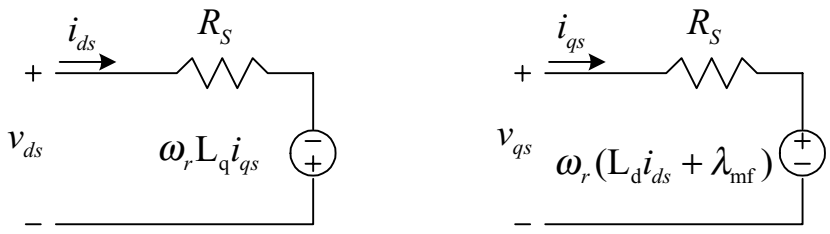

Fig. 4.1. The d- and q- axis steady state equivalent circuits in the rotor reference frame of an IPMSM.

following equation [13]:

$$f(i_{ds},\ i_{qs}) = 2(\mathrm{L_q} - \mathrm{L_d})\ i_{ds} - \lambda_{\mathrm{mf}} + \sqrt{\lambda_{\mathrm{mf}}^2 + 4(\mathrm{L_q} - \mathrm{L_d})^2 i_{qs}^2} = 0 \tag{4.1}$$

In particular, when the maximum line current magnitude $\mathrm{I_{sm}}$ is imposed, namely

$$i_{ds}^2 + i_{qs}^2 = \mathrm{I_{sm}^2} \tag{4.2}$$

Then, from (4.1) and (4.2) one can obtain the maximum available torque, T_{eM}, as follows:

$$T_{eM} = 0.75\,\mathrm{p}\,[\lambda_{\mathrm{mf}} + (\mathrm{L_d} - \mathrm{L_q})\, I_{dsM}]\, I_{qsM} \tag{4.3}$$

where

$$I_{dsM} \triangleq \frac{\lambda_{\mathrm{mf}} - \sqrt{\lambda_{\mathrm{mf}}^2 + 8(\mathrm{L_q} - \mathrm{L_d})^2 \mathrm{I_{sm}^2}}}{4(\mathrm{L_q} - \mathrm{L_d})} \tag{4.4}$$

$$I_{qsM} \triangleq \sqrt{\mathrm{I_{sm}^2} - I_{dsM}^2} \tag{4.5}$$

Also, the corresponding angular speed, namely ω_{rM} can be calculated by substituting equations (2.6), (2.7), (4.4), and (4.5) into the following voltage boundary equation

$$(\mathrm{R_s} I_{dsM} - \omega_{rM} \mathrm{L_q} I_{qsM})^2 + \left[\mathrm{R_s} I_{qsM} + \omega_{rM} (\mathrm{L_d} I_{dsM} + \lambda_{\mathrm{mf}})\right]^2 = \mathrm{V_{sm}^2} \tag{4.6}$$

Thus, whenever there exists a speed deviation during the control process, the maximum torque T_{eM} can be applied to achieve the fastest response.

Next, in order to achieve a linear control law, a virtual control u^*, corresponding to a

torque command T_e^*, can be defined as follows:

$$u^* \triangleq \frac{T_e^*}{\mathrm{K_{tM}}} = \frac{0.75\ \mathrm{p}\ [\lambda_{\mathrm{mf}} + (\mathrm{L_d}\text{-}\mathrm{L_q})\ i_{ds}^*]\ i_{qs}^*}{\mathrm{K_{tM}}} \tag{4.7}$$

where constant $\mathrm{K_{tM}}$ is chosen to be

$$\mathrm{K_{tM}} \triangleq \frac{T_{eM}}{\mathrm{I_{sm}}} \tag{4.8}$$

As will be clear from later sections, the same constant, $\mathrm{K_{tM}}$, is used not only in the constant torque limit range but also in the entire field weakening range. In fact, the discovery of the proposition of the constant $\mathrm{K_{tM}}$ is inspired from the proposed LTC control strategy of the IPMSM drives as described in Chapter 2. For convenient explanation of the proposed linear maximum torque per ampere (LMTPA) control, define Region I as the constant torque limit region where $\omega_r < \omega_{rM}$. Hence, in this region, if a torque command $T_e^*(=\mathrm{K_{tM}}\ u^*)$ is given, then the corresponding d-axis current command (i_{ds}^*) can be solved from the following polynomial equation

$$\begin{aligned} &P_1(i_{ds}^*) \triangleq \\ &(\mathrm{L_d}\text{-}\mathrm{L_q})^3\ i_{ds}^{*\,4} + 3\ (\mathrm{L_d}\text{-}\mathrm{L_q})^2\ \lambda_{\mathrm{mf}}\ i_{ds}^{*\,3} + 3\ (\mathrm{L_d}\text{-}\mathrm{L_q})\ \lambda_{\mathrm{mf}}^2 i_{ds}^{*\,2} \\ &+\lambda_{\mathrm{mf}}^3 i_{ds}^* - \frac{16}{9\mathrm{p}^2}(\mathrm{L_d}\text{-}\mathrm{L_q})\mathrm{K_{tM}^2} u^{*2} = 0 \end{aligned} \tag{4.9}$$

which is obtained by substituting

$$i_{qs} = \frac{T_e^*}{0.75\mathrm{p}[\lambda_{\mathrm{mf}} + (\mathrm{L_d}\text{-}\mathrm{L_q})i_{ds}^*]} = \frac{\mathrm{K_{tM}}\ u^*}{0.75\mathrm{p}[\lambda_{\mathrm{mf}} + (\mathrm{L_d}\text{-}\mathrm{L_q})i_{ds}^*]} \tag{4.10}$$

into (4.1). Similarly, by substituting

$$i_{ds} = (\frac{\mathrm{K_{tM}}\ u^*}{0.75\mathrm{p}} - \lambda_{\mathrm{mf}}\ i_{qs}^*)/((\mathrm{L_d}\text{-}\mathrm{L_q})\ i_{qs}^*) \tag{4.11}$$

into (4.1) one can obtain the following relation

$$P_2(i_{qs}^*) \triangleq 9\mathrm{p}^2(\mathrm{L_d}\text{-}\mathrm{L_q})^2\ i_{qs}^{*\,4} + 12\mathrm{p}\ \mathrm{K_{tM}}\ \lambda_{\mathrm{mf}}\ u^* i_{qs}^* - 16\mathrm{K_{tM}^2}\ u^{*2} = 0 \tag{4.12}$$

And the corresponding q-axis current command i_{qs}^* can be solved from (4.12). Although the orders of (4.9) and (4.12) look rather high, as will be clear in later implementation example, a second order polynomial approximation is in fact accurate enough. The desired i_{ds}^* and i_{qs}^* can be obtained easily by using any available commercial numerical program with zero initial values. For clarity, the trajectory of (4.1) on the i_{ds}-i_{qs} plane, namely AIO curve, is shown in Fig. 4.2 where the current limit curve and one constant torque curve together with five voltage limit curves are also shown on the same figure. In summary, in Region I, given a torque command T_e^*, one can get the corresponding virtual control u^*. Then, from u^* one can obtain the corresponding i_{ds}^* and i_{qs}^* from (4.9) and (4.12) respectively. Although the generated torque command T_e^* as in (2.5) is still nonlinear to i_{ds}^* and i_{qs}^*, but it is now proportional to the virtual control u^* as in (4.7). Thus, excluding the inner current loop control, the outer loop controller can be easily designed by using any existing linear control strategy directly. Since the AIO curve in Fig. 4.2 is identical with the maximum torque per ampere control [13], the proposed linear control can achieve the same dynamic performance as in [13].

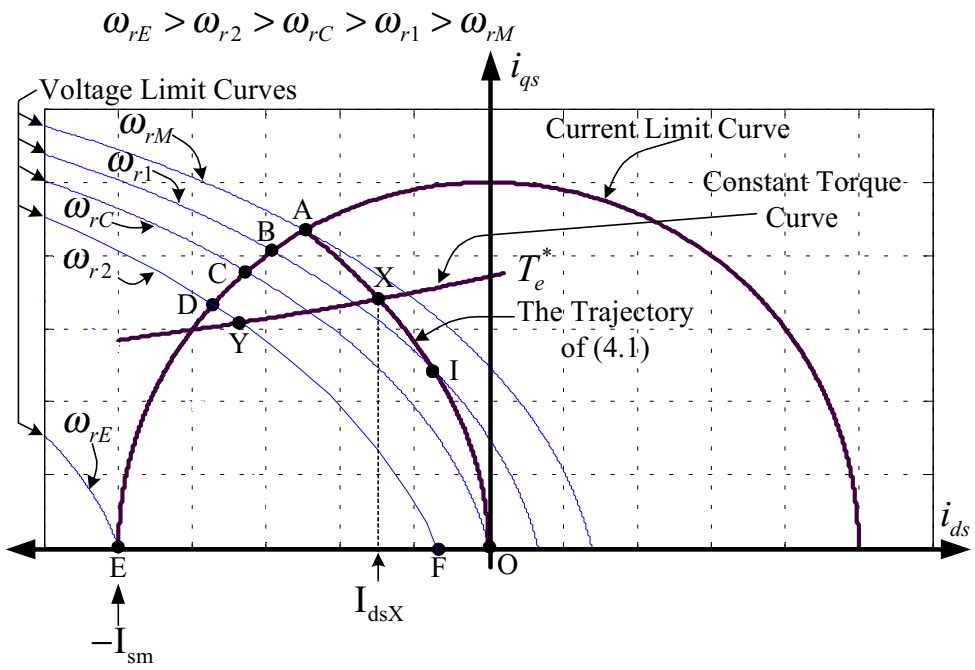

Fig. 4.2. The trajectories of (4.1), the current limit curve, one constant torque curve, and five voltage limit curves on i_{ds}-i_{qs} plane for an IPMSM.

4.3 Extension of the Proposed LMTPA to the Field Weakening Region

From the previous section, it is seen that during acceleration, for $\omega_r < \omega_{rM}$, one can choose the maximum torque T_{eM} to achieve the fastest response. However, when $\omega_r > \omega_{rM}$, due to the current and voltage constraints of (2.21) and (2.22), the maximum torque (T_{eM}) can not be achieved. The traditional control strategy is simply to reduce the magnetic field intensity by applying negative i_{ds} resulting in the so called field weakening control. As can be observed from Fig. 4.2, as far as the current constraint is concerned, the field weakening region is bounded by the ABCDE curve, the AIO curve, and the EO axis. In particular, four points (namely B, C, D, and E) are also marked in Fig. 4.2, where the voltage limit is also

imposed on, namely

$$v_{ds}^2 + v_{qs}^2 = \mathrm{V}_{\mathrm{sm}}^2 \tag{4.13}$$

By substituting (2.6) and (2.7) into (4.13) yields

$$\begin{aligned} g(i_{ds}, i_{qs}, \omega_r) \triangleq & (\mathrm{R_S}\, i_{ds} - \omega_r \mathrm{L_q}\, i_{qs})^2 + \\ & (\mathrm{R_S}\, i_{qs} + \omega_r \mathrm{L_d}\, i_{ds} + \omega_r \lambda_{\mathrm{mf}})^2 - \mathrm{V}_{\mathrm{sm}}^2 = 0 \end{aligned} \tag{4.14}$$

Thus, from (4.14), it is seen that when $i_{ds} = i_{qs} = 0$, then one can obtain the corresponding speed, called the critical angular frequency ω_{rC} that is the same as (3.3) for the same IPMSM and the drive specifications. Similarly, from (4.14), when $i_{ds} = \text{-}\mathrm{I}_{\mathrm{sm}}$ and $i_{qs} = 0$ then one can obtain the corresponding speed, called the extreme angular frequency ω_{rE} that is also the same as (3.4) for the same IPMSM and the drive specifications.

The corresponding operating points of ω_{rC} and ω_{rE} on the $i_{ds} - i_{qs}$ plane are just the C and E points marked in Fig. 4.2. Also, from (3.4), one can see that to get positive value of ω_{rE}, it is necessary that λ_{mf} is greater than $\mathrm{L_d I_{sm}}$. Indeed, in practical operation situations, $\mathrm{L_d}\left|i_{ds}\right|$ is less than λ_{mf}. Further examination of Fig. 4.2 reveals that when the motor speed $\omega_r \in (\omega_{rM}, \omega_{rC})$, then the voltage bound curve of (4.14) will intersect with the AIO curve. For example, Fig. 4.2 shows a voltage bound curve for $\omega_r = \omega_{r1}$, and the corresponding intersecting point is I. In other words, for each given $\omega_r \in (\omega_{rM}, \omega_{rC})$, the corresponding boundary currents i_{dsb} and i_{qsb} of point I can be solved from the following system of polynomials, namely (4.1) and (4.14)

$$f(i_{dsb}, i_{qsb}) = 0 \tag{4.15}$$

$$g(i_{dsb}, i_{qsb}, \omega_r) = 0 \tag{4.16}$$

Hence, the corresponding electromagnetic torque bound and virtual control bound, namely T_{eb} and u_b, can be defined as follows

$$T_{eb} \triangleq 0.75\,\mathrm{p}\,[\lambda_{\mathrm{mf}} + (\mathrm{L_d} - \mathrm{L_q})\, i_{dsb}]\, i_{qsb} \tag{4.17}$$

$$u_b \triangleq \frac{T_{eb}}{\mathrm{K_{tM}}} \tag{4.18}$$

Now it is quite clear from Fig. 4.2 that when $\omega_r = \omega_{r1}$ and $T_e^* < T_{eb}$, then despite that ω_{r1} is located in the conventional field weakening region, one can still use the maximum torque per ampere control, namely corresponding to the curve IO portion of Fig. 4.2, to achieve the minimum copper loss. Also the corresponding u^* as well as i_{ds}^* and i_{qs}^* remains the same as that obtained from (4.9) and (4.12). However, when $T_e^* > T_{eb}$, due to the voltage constraint, it is not possible to achieve the conventional maximum torque per ampere control. Therefore, the proposed control strategy chooses i_{ds}^* and i_{qs}^*, for a given T_e^* (and $u^* = \frac{T_e^*}{\mathrm{K_{tM}}}$), as the intersection point of the torque command equation (2.5) and the voltage limit equation (4.14). Similar to the previous constant torque limit control, for convenience, by using (2.5) one can either eliminate i_{qs}^* to yield

$$\begin{aligned} P_{1w}(i_{ds}^*) = &\left[R_s i_{ds}^* - \omega_r \mathrm{L_q} \frac{\mathrm{K_{tM}} u^*}{0.75\mathrm{p}\left[\lambda_{\mathrm{mf}} + (\mathrm{L_d} - \mathrm{L_q}) i_{ds}^*\right]} \right]^2 + \\ &\left[\frac{R_s \mathrm{K_{tM}} u^*}{0.75\mathrm{p}\left[\lambda_{\mathrm{mf}} + (\mathrm{L_d} - \mathrm{L_q}) i_{ds}^*\right]} + \omega_r (\mathrm{L_d} i_{ds}^* + \lambda_{\mathrm{mf}}) \right]^2 - \mathrm{V_{sm}^2} = 0 \end{aligned} \tag{4.19}$$

or eliminate i_{ds}^* to yield

$$P_{2w}(i_{qs}^*) = [\mathrm{R_s}(\frac{\mathrm{K_{tM}}\ u^*}{0.75\mathrm{p}} - \lambda_{\mathrm{mf}}\ i_{qs}^*)/((\mathrm{L_d}\text{-}\mathrm{L_q})\ i_{qs}^*) - \omega_r \mathrm{L_q} i_{qs}^*]^2 +$$
$$[\mathrm{R_s} i_{qs}^* + \omega_r(\mathrm{L_d}(\frac{\mathrm{K_{tM}}\ u^*}{0.75\mathrm{p}} - \lambda_{\mathrm{mf}}\ i_{qs}^*)/((\mathrm{L_d}\text{-}\mathrm{L_q})\ i_{qs}^*) + \lambda_{\mathrm{mf}}\ )]^2 - \mathrm{V_{sm}^2} = 0 \quad (4.20)$$

In summary, for $\omega_r \in (\omega_{rM}, \omega_{rC})$, if $u^* < u_b$ (or equivalently $T_e^* < T_{eb}$), then the previous maximum torque per ampere control can be applied. If $u^* \geq u_b$, then the field weakening control which is obtained from (4.19) and (4.20) should be applied. Since there are two control modes applicable in this speed range, it is called the partial field weakening region (Region II). It is worth mentioning that within the partial field weakening region, the virtual control bound u_b is not a constant. It is varied with motor speed ω_r. For reference, Fig. 4.3 also shows the trajectory of a virtual control bound within the partial field weakening region as an illustration. Furthermore, for $\omega_r \in (\omega_{rC}, \omega_{rE})$, it is seen from Fig. 4.2 that it is not possible to have an intersection point for (4.1) and (4.14). Thus, for each torque command T_e^* (or equivalently u^*), the same field weakening control equations, (4.19) and (4.20) are directly applied to find the corresponding i_{ds}^* and i_{qs}^*. Therefore, in this speed region, it is called the full field weakening region (Region III). For reference, Fig. 4.4 shows a schematic diagram for the maximum available torque with respect to the whole speed range. In fact, one of the characteristics of the proposed control strategy is that under transient condition, no matter the operation speed is located in which region, the maximum torque capability can always be applied to achieve the fastest response. From previous results, the proposed control strategy has been shown to be a linear one over the entire speed region. Also, for

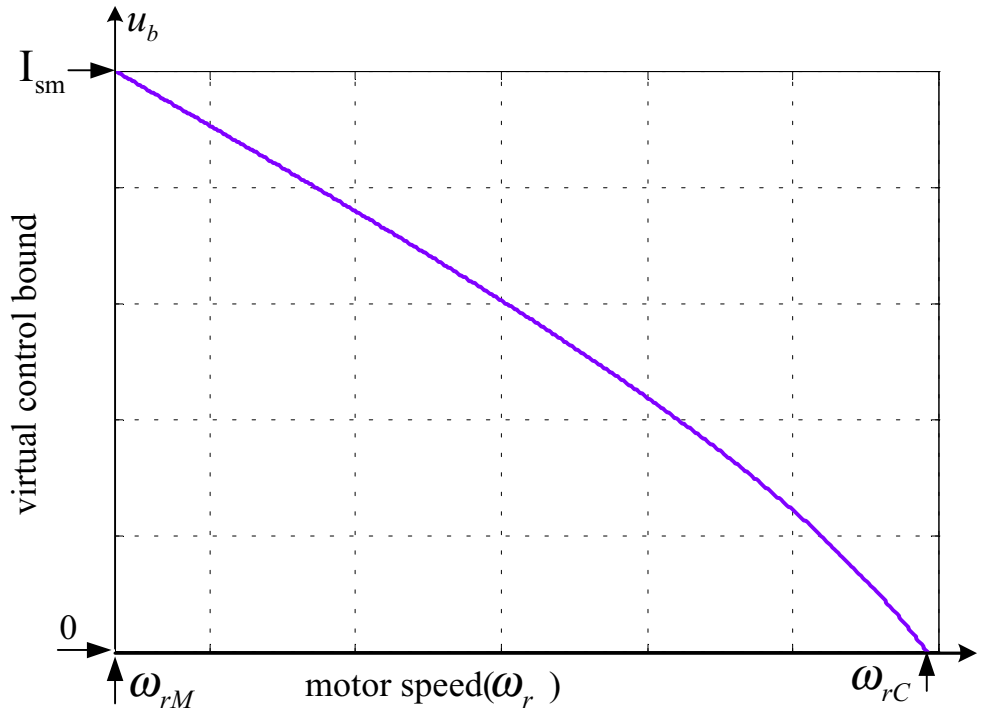

Fig. 4.3. Graphical illustration of the virtual control bound to motor speed curve for $\omega_{rM} \le \omega_r \le \omega_{rC}$.

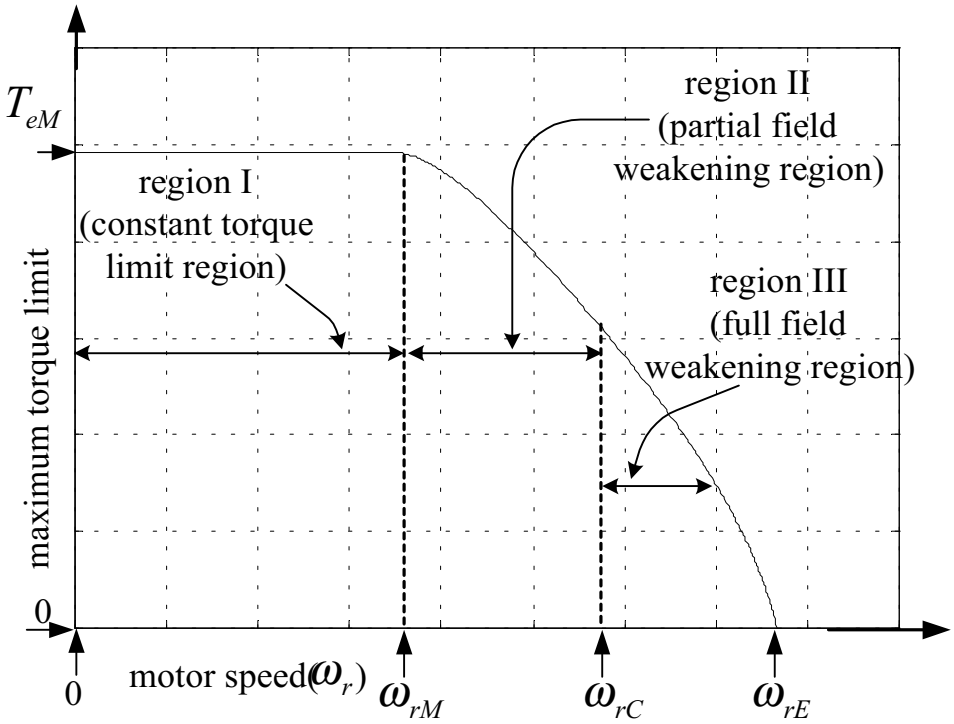

Fig. 4.4. Illustration of the maximum torque limit to motor speed curve and three operation regions for the proposed LMTPA control.

Region I and portion of Region II, the proposed control is identical with the existing maximum torque per ampere control to achieve minimum copper loss.

It remains to prove that the proposed control in the field weakening range can also achieve the minimum copper loss. By using (2.5), one can get

$$\begin{aligned} i_{ds}^2 + i_{qs}^2 &\triangleq h(i_{ds}) \\ &= i_{ds}^2 + \left(\frac{T_e}{0.75\mathrm{p}\left[\lambda_{\mathrm{mf}} + (\mathrm{L_d} - \mathrm{L_q}) i_{ds}\right]}\right)^2 \end{aligned} \tag{4.21}$$

It follows from (4.21) that

$$\frac{d\ h(i_{ds})}{d\ i_{ds}} = 2i_{ds} - \frac{1.5\mathrm{p}T_e^2(\mathrm{L_d} - \mathrm{L_q})}{[0.75\mathrm{p}(\lambda_{\mathrm{mf}} + (\mathrm{L_d} - \mathrm{L_q}) i_{ds})]^3} \tag{4.22}$$

Equation (4.22) can be further simplified by substituting (2.5) to obtain

$$\frac{dh(i_{ds})}{d\ i_{ds}} = 2i_{ds} - \frac{2i_{qs}^2(\mathrm{L_d} - \mathrm{L_q})}{\lambda_{\mathrm{mf}} + (\mathrm{L_d} - \mathrm{L_q}) i_{ds}} \tag{4.23}$$

It follows from (4.23) that in case the derivative is set equal to zero, one can obtain the familiar $i_{ds} \sim i_{qs}$ relation for the maximum torque per ampere control [13] as follows:

$$i_{ds} = \frac{\lambda_{\mathrm{mf}} - \sqrt{\lambda_{\mathrm{mf}}^2 + 4(\mathrm{L_d} - \mathrm{L_q})^2 i_{qs}^2}}{2(\mathrm{L_q} - \mathrm{L_d})} \tag{4.24}$$

Thus, when the proposed field weakening control is applied in either Region III or Region II for each $T_e^* > T_{eb}$, it can be observed from Fig. 4.2 that the corresponding constant torque curve intersects with AIO curve at point X. Assume the corresponding d-axis current is

denoted as $\mathrm{I}_{\mathrm{dsX}}$. Then from Fig. 4.2, one can see that

$$i_{ds}^{*} < \mathrm{I}_{\mathrm{dsX}} \tag{4.25}$$

It follows from (4.23) and (4.25) that

$$\frac{d\ h(i_{ds})}{d\ i_{ds}}\Big|_{i_{ds}=i_{ds}^{*}} < 0,\ \ i_{ds}^{*} \in (-\mathrm{I}_{\mathrm{sm}},\ \mathrm{I}_{\mathrm{dsX}}) \tag{4.26}$$

In other words, for a fixed positive torque command T_e^*, the corresponding $h(i_{ds}^*) = i_{ds}^{*\,2} + i_{qs}^{*\,2}$ is a monotonically decreasing function with increasing i_{ds}^* as long as (4.25) is satisfied. As an illustration example, consider the example as shown in Fig. 4.2 where a constant torque curve marked with T_e^* and a voltage limit curve with ω_{r2} are shown. One can see that the constant T_e^* curve intersects with the AIO curve at X point and intersects with the constant ω_{r2} voltage limit at Y point. Hence, according to (4.26), one can see as one moves from point Y to X, i.e., as the corresponding i_{ds} is increasing, the corresponding squared current magnitude, or $h(i_{ds})$ equivalently, will decrease monotonically. This implies that the corresponding i_{ds}^* of Y point is the largest one within the feasible constant torque trajectory. Hence, the proposed linear control can indeed achieve the minimum copper loss in the field weakening region.

Finally, consider the transient control. For example, during the motor starting stage, since $\omega_r < \omega_{rM}$, the maximum torque (T_{eM}) can be applied to achieve the fastest response. However, when the motor speed is greater than ω_{rM}, the maximum torque T_{eM} cannot be

achieved. For the proposed LMTPA control and for each ω_r, the corresponding maximum torque, called T_{eMF}, can be obtained by first finding the corresponding d- and q-axis currents, namely I_{dsMF} and I_{qsMF} from (4.2) and (4.14)

$$I_{dsMF}^2 + I_{qsMF}^2 = \mathrm{I}_{\mathrm{sm}}^2 \tag{4.27}$$

$$g(I_{dsMF}, I_{qsMF}, \omega_r) = 0 \tag{4.28}$$

Then, the maximum torque and maximum virtual control becomes

$$T_{eMF}\Big|_{\omega_r} = 0.75\mathrm{p}\left[\lambda_{\mathrm{mf}} + (\mathrm{L_d}\text{-}\mathrm{L_q})\, I_{dsMF}\right] I_{qsMF} \tag{4.29}$$

$$u_{MF}\Big|_{\omega_r} = \frac{T_{eMF}\Big|_{\omega_r}}{\mathrm{K_{tM}}} \tag{4.30}$$

It should be mentioned that both I_{dsMF} and I_{qsMF} are functions of ω_r for $\omega_r \in (\omega_{rM}, \omega_{rE})$.

4.4 Implementation and Experimental Results of the Proposed LMTPA Control

For convenient reference, an implementation block diagram of the speed control system according to the proposed LMTPA control is shown in Fig. 4.5 as an illustrative example. It is seen from Fig. 4.5 that ω_r^* is a speed command. The signals of i_{as} and i_{bs} are the line currents of phases a and b respectively. The pulse signals of A, B, and Z are the outputs of the incremental encoder where A and B are two sequences of pulses with variable frequencies and fixed phase shifts of 90 degrees. The Z signal is used for resetting when the rotor of the motor revolves o ne cycle, a signal pulse will appear in Z. Except for the adaptive limiter

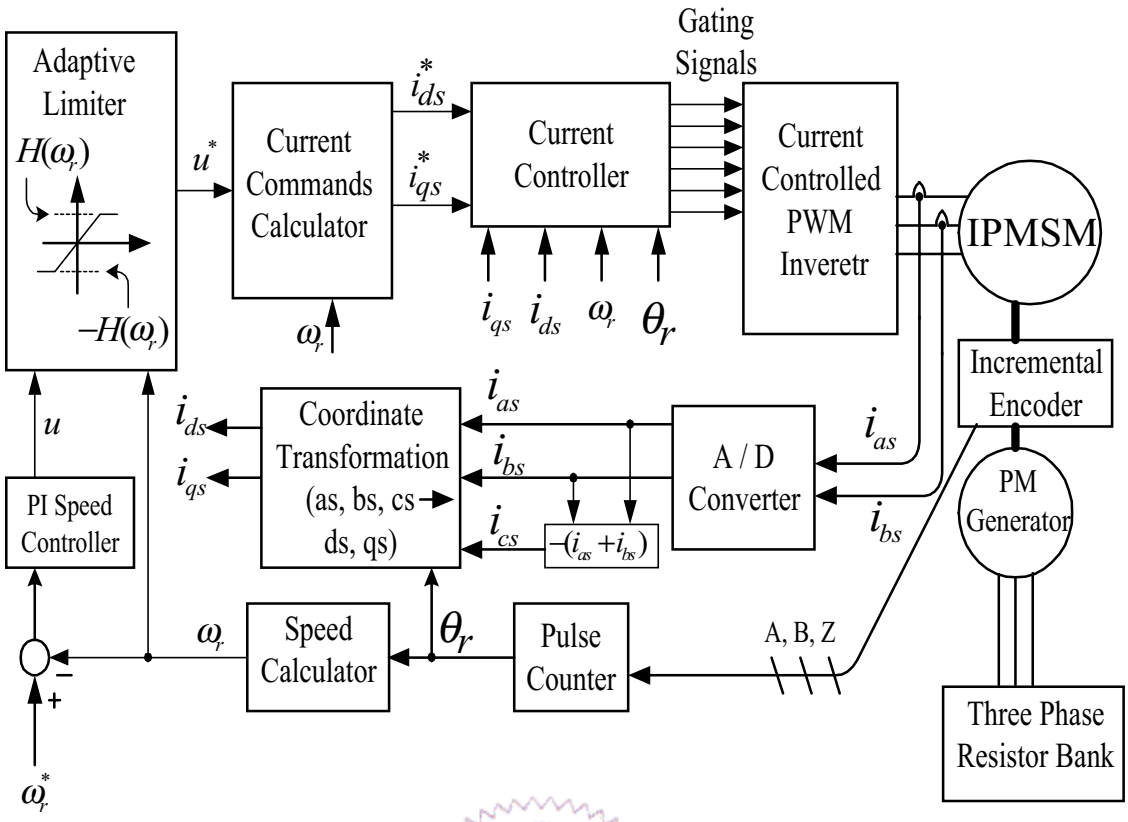

Fig. 4.5. Block diagram of the developed IPMSM drive system.

block and the current command calculator, the other blocks are quite typical and will not be explained further. Actually, except for the adaptive limiter block and the current commands calculator block, the functions of the other blocks are the same as that in Fig. 3.4. The function of the adaptive limiter block in Fig. 4.5 is the modified version of the torque limiter block in Fig. 3.4. The explanation of the function of the adaptive limiter will be presented as follows. From the proposed control strategy it is seen that for $\omega_r \le \omega_{rM}$, the maximum virtual control available is chosen to be

$$u_M = \frac{T_{eM}}{K_{tM}} = I_{sm},\ \omega_r \le \omega_{rM} \tag{4.31}$$

Also, for $\omega_r \in (\omega_{rM}, \omega_{rE})$, the maximum virtual control available is u_{MF} from (4.30). For

easy implementation, one can define an adaptive limiter with the following adaptive upper bound

$$H(\omega_r) \triangleq \begin{cases} u_M = I_{sm}, 0 \le \omega_r \le \omega_{rM} \\ u_{MF}\big|_{\omega_r}, \omega_{rM} < \omega_r < \omega_{rE} \end{cases} \tag{4.32}$$

The shape of the adaptive upper bound $H(\omega_r)$ over the entire speed range is the same as in Fig. 4.4 except that the unit of the vertical axis is ampere. Furthermore, although the shape of the adaptive upper bound $H(\omega_r)$ in (4.32) is similar to that of $f(\omega_r)$ in (3.9), but both $H(\omega_r)$ and $f(\omega_r)$ are two different functions. They are based on two different torque control strategies. Of course, when the output of the speed controller is not saturated, then the corresponding virtual control u^* is the same as the original u in this linear control region as shown in Fig. 4.5. Next, consider the current commands calculator. Fig. 4.6 shows the detailed flowchart of how to calculate the desired i_{ds}^* and i_{qs}^* for each virtual control u^* in different speed regions according to the proposed control strategy. One can see that the function of the current commands calculator block in Fig. 4.5 is a modified version of the control mode detector block in Fig. 3.4. Or equivalently to say, the flowchart of the current commands calculator as shown in Fig. 4.6 is a modified version of that of the control mode detector in Fig. 3.6. Although the signal flow logic of both Fig. 3.6 and Fig. 4.6 looks quite similar, but all the parameters of the equations are entirely different. However, for simplifying the complicated calculation, the solutions of (4.9) and (4.12) are calculated offline over the entire range of u^*. Then the equations of i_{ds}^* and i_{qs}^* can be obtained by using approximated second order polynomials with least square error approximation method. These two equations are listed as follows for the constant torque limit control:

$$i_{ds}^{*} = \mathrm{m}_1 (u^{*})^2 + \mathrm{m}_2 u^{*} + \mathrm{m}_3 \tag{4.33}$$

$$i_{qs}^{*} = \mathrm{m}_4 (u^{*})^2 + \mathrm{m}_5 u^{*} + \mathrm{m}_6 \tag{4.34}$$

where m_1 to m_6 are real constants. Similarly, for each $\omega_r \in (\omega_{rM}, \omega_{rE})$ in the field weakening control, the solutions of (4.19) and (4.20) can be approximated by the following expressions:

$$i_{ds}^{*} = w_1 (u^{*})^2 + w_2 u^{*} + w_3 \tag{4.35}$$

$$i_{qs}^{*} = w_4 (u^{*})^2 + w_5 u^{*} + w_6 \tag{4.36}$$

Since the values of w_1 to w_6 in (4.35) and (4.36) now varies with ω_r for $\omega_r \in (\omega_{rM}, \omega_{rE})$, the second order polynomials with least square error approximation can also be used to find the equations of w_k, $k = 1, 2, ..., 6$ as

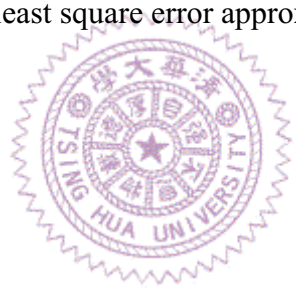

$$w_k = c_{k1}\omega_r^2 + c_{k2}\omega_r + c_{k3} \tag{4.37}$$

with c_{kj}, $k = 1, 2, ..., 6$, $j = 1, 2, 3$ being real constants. From actual experiments, it is found that, with the above approximations, the errors between the actual current commands and the approximated current commands for both d- and q-axis are less than 1%, but the calculation time is greatly reduced.

In order to verify the feasibility of the proposed control strategy, a prototype is constructed according to the block diagram of Fig. 4.5 by using a fixed-point DSP TMS320F240. The sampling time periods for the current controller and the speed controller are chosen to be 0.1 msec and 1 msec respectively. The tested IPMSM, a prototype designed in [67], has the parameters of motor D as shown in Table 2.1. The corresponding ω_{rM} and

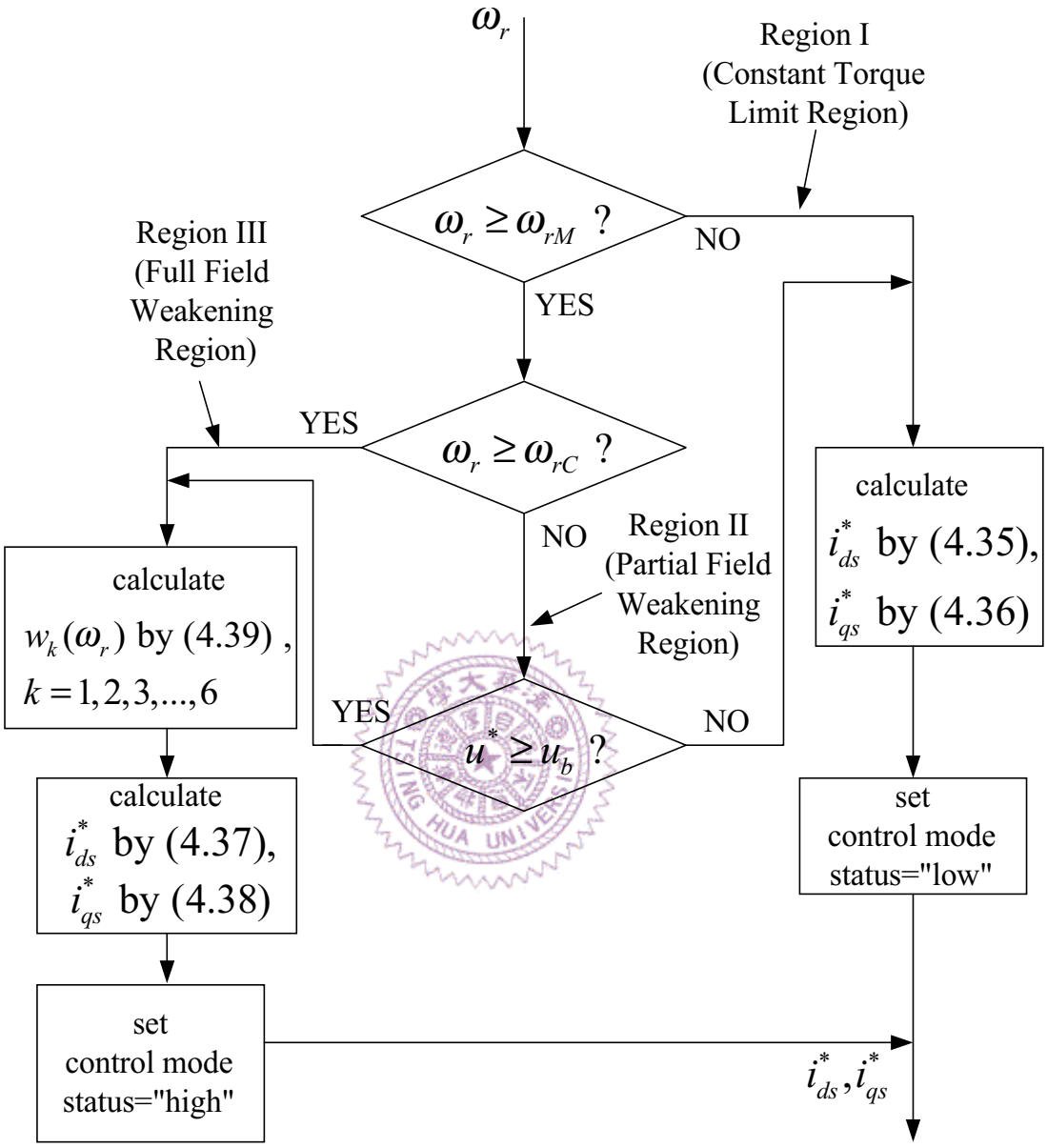

Fig. 4.6. The flowchart of the current commands calculator as reference to Fig. 4.5.

ω_{rC} are found to be 3235 rpm and 3790 rpm from (4.6) and (3.3) respectively. Similarly, the I_{dsM} and I_{qsM} are –6.6(A) and 24.1(A) from (4.4) and (4.5) respectively.

Four experimental results are presented to illustrate the characteristics of the developed drive system. To demonstrate the smooth transitions between the constant torque limit control mode and the field weakening control mode in the partial field weakening region, first consider the case of applying a step command of ω_r^*=3650 rpm to the tested IPMSM drive starting from rest at t=0 sec and with lighter load such that the control is settled down to a constant torque limit control. Fig. 4.7 shows the d- and q-axis current responses, speed response, and the control mode status to show the transition between the constant torque limit control mode and the field weakening control mode. As can be observed from Fig. 4.7, when the motor is accelerating up to ω_{rM} (=3235 rpm), the motor is operated in Region I and the responses of i_{ds} and i_{qs} indeed follow approximately i_{dsM} and i_{qsM} respectively. Also the corresponding control mode status in Fig. 4.7 is at the low level. As soon as ω_r is greater than ω_{rM}, the motor is then operated in Region II. The responses of i_{ds} and i_{qs} decrease with the increase of ω_r until the motor speed ω_r reaches the speed command ω_r^*=3650 rpm. On the other hand, the control mode status in Fig. 4.7 has changed to the high level (the field weakening control mode) at $\omega_r = \omega_{rM}$=3235 rpm. This field weakening control mode persists until about t=1.0 sec, then the motor speed reaches the steady state speed ω_r =3650 rpm and the resulting control becomes the MTPA control. Meanwhile, the control mode status shows a second transition from the high level to the low level. It can be checked that the motor load torque T_L (approximately 0.9 Nm at 3650 rpm) is less than $K_{tM}u_b$ (=1.7 Nm) at ω_r =3650 rpm.

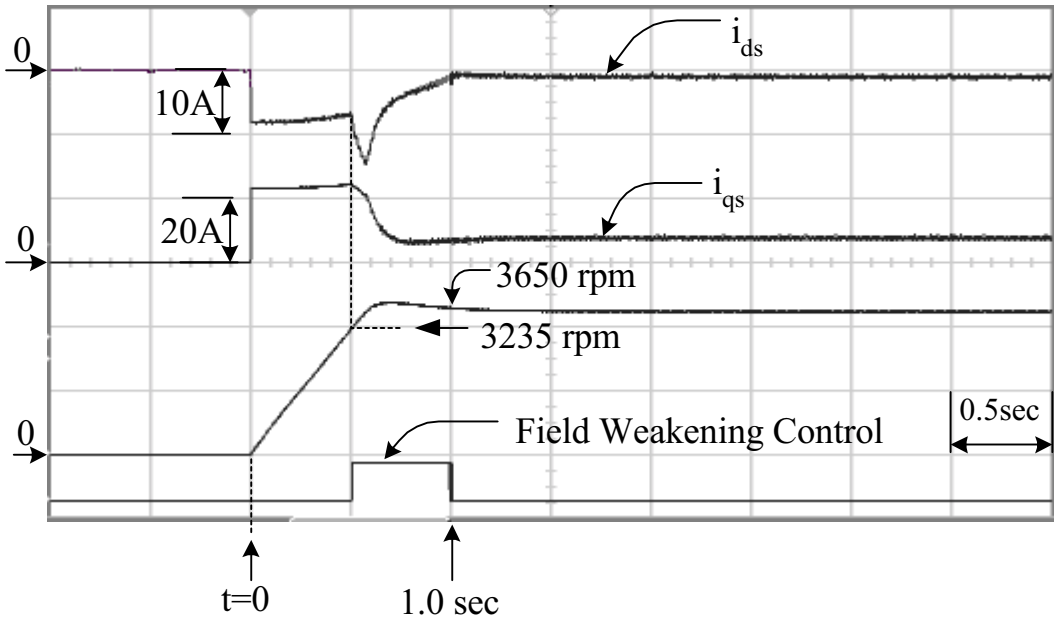

Fig. 4.7. Experimental results of i_{ds}, i_{qs}, and motor speed responses for the proposed control in the partial field weakening region under lighter load.

The second test condition is almost the same as the first one except that a heavier load is applied such that the final control is settled down to the field weakening control. Fig. 4.8 shows the d- and q-axis current responses, speed response, and the corresponding control mode status for the same step speed command as Fig. 4.7. One can see that the control mode status in Fig. 4.8 shows only one transition from the low level to the high level, i.e. remaining in the field weakening control mode. It can also be checked that this load torque T_L (approximately 3.0 Nm at 3650 rpm) is greater than the corresponding $K_{tM}u_b$ (=1.7 Nm) at ω_r =3650 rpm.

Thirdly, to demonstrate the operation mode in Region III, a step command of ω_r^*=4200 rpm which is greater than ω_{rC} =3790 rpm is applied to the IPMSM drive starting from rest at t=0 sec. Fig. 4.9 shows the corresponding d- and q-axis current responses, speed response, and the control mode status. As shown in Fig. 4.9, when the motor speed reaches

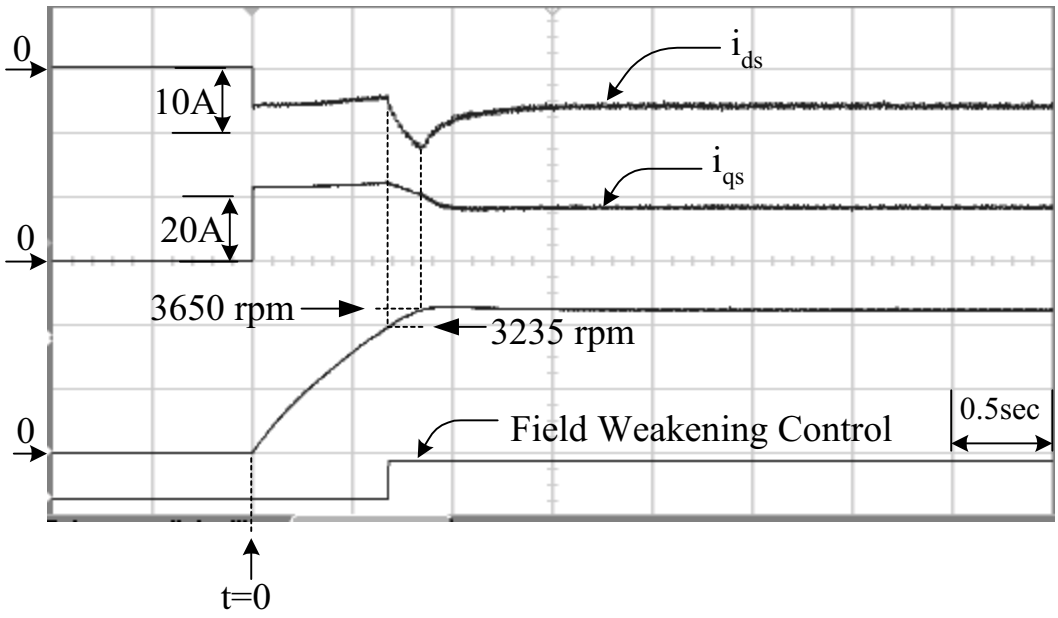

Fig. 4.8. Experimental results of i_{ds}, i_{qs}, and motor speed responses for the proposed control in the partial field weakening region under heavier load.

$\omega_r = \omega_{rM}$ =3235 rpm the control mode status also indicates a transition from low level to high level. When $\omega_r > \omega_{rM}$, then I_{dsMF} and I_{qsMF} both start decreasing until the motor speed ω_r is greater than the speed command ω_r^* =4200 rpm at about t=0.73 sec. For t≥0.73 sec, the magnitudes of i_{ds} and i_{qs} gradually decrease to the steady state values. However, since the motor speed is greater than ω_{rC} (=3790 rpm), the steady state operation mode is still kept in the field weakening control mode as can be observed from the control mode status of Fig. 4.9. For reference, Fig. 4.10 also shows the corresponding trajectory on the i_{ds}-i_{qs} plane corresponding to the time responses of Fig. 4.9. It is seen that the current vector starts from zero to point A quickly and then the current trajectory moves approximately along the current limit curve until point D where the motor speed reaches the command speed. Finally, the magnitude of the current vector decreases and then settles down to the steady state operating point to match the corresponding load torque.

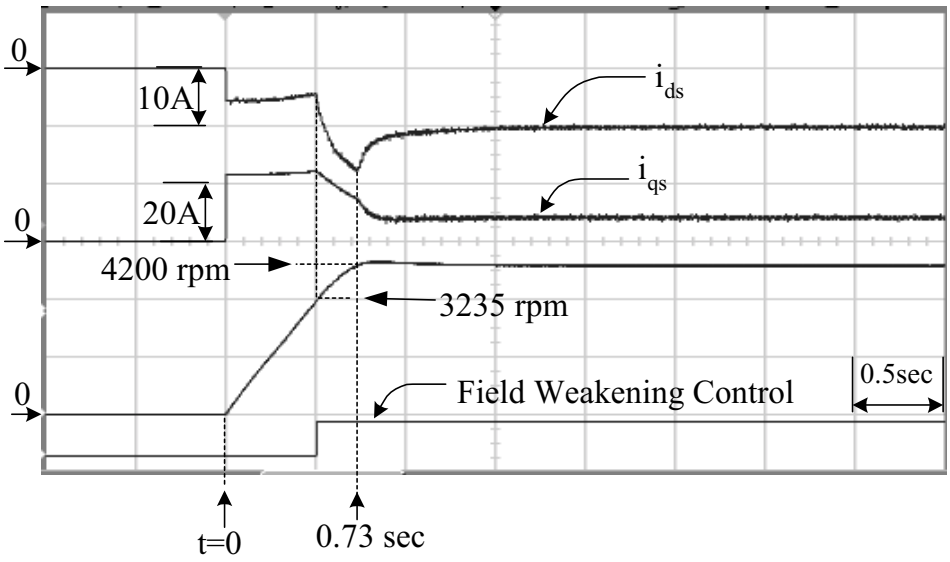

Fig. 4.9. Experimental results of i_{ds}, i_{qs}, and motor speed responses for the proposed control in the full field weakening region.

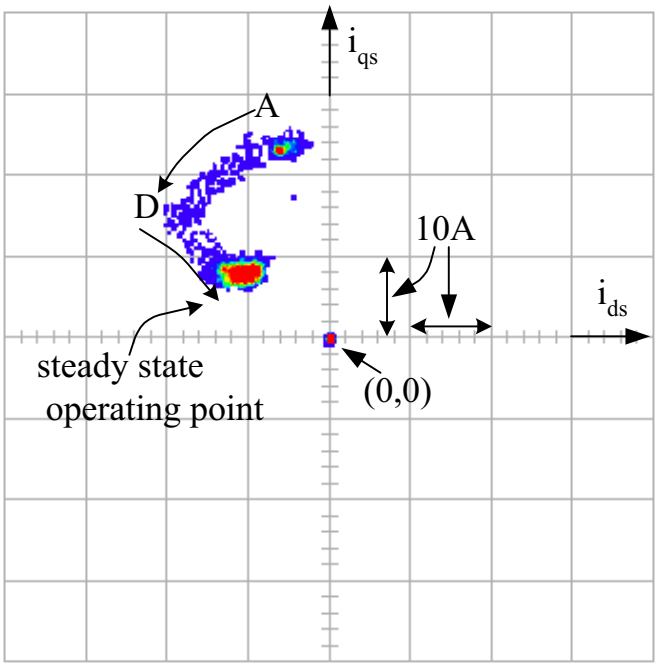

Fig. 4.10. The i_{ds}-i_{qs} plot corresponding to Fig. 4.9.

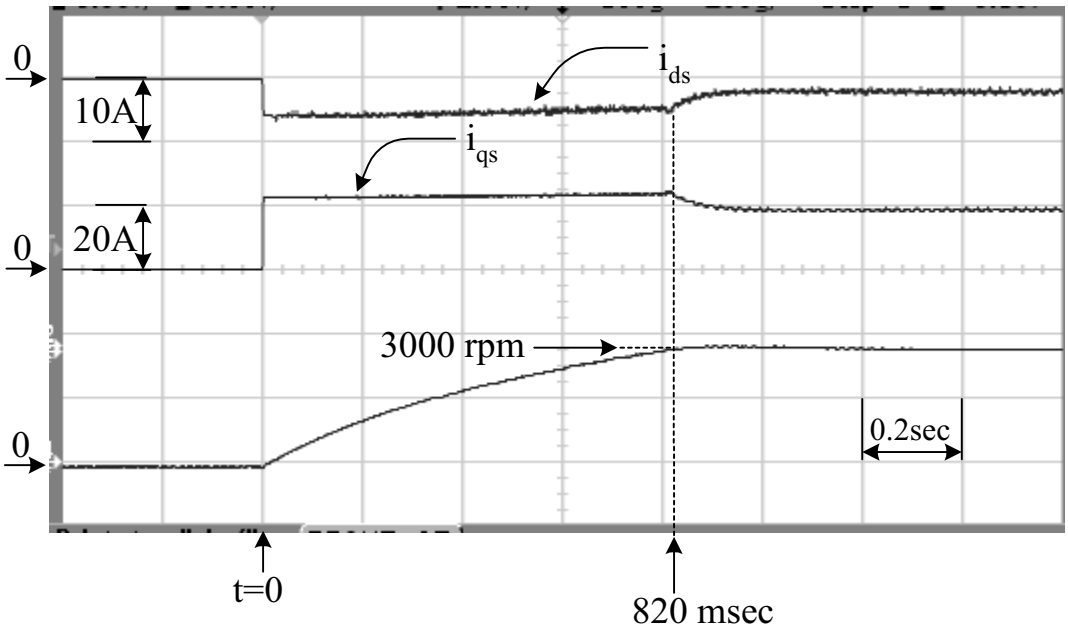

Fig. 4.11. Experimental results of i_{ds}, i_{qs}, and motor speed responses by the proposed LMTPA control.

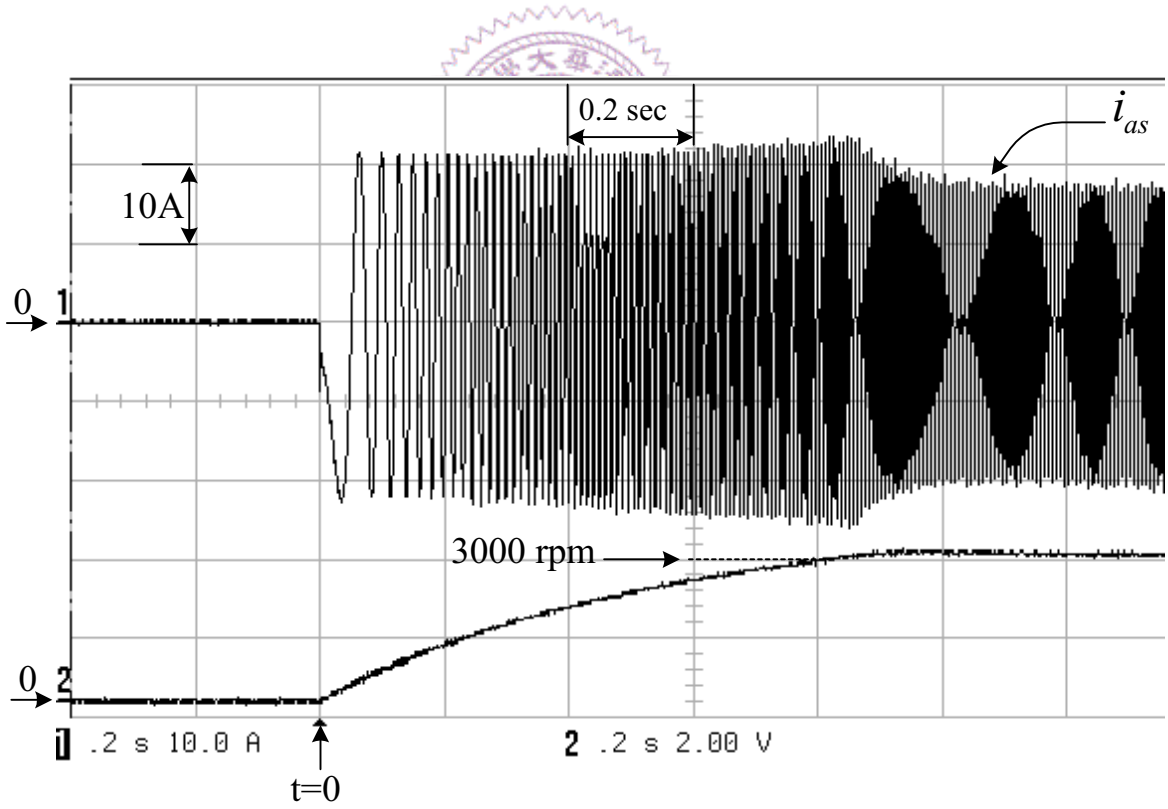

Fig. 4.12. The waveforms of the phase-a current response and the speed response corresponding to Fig. 4.11.

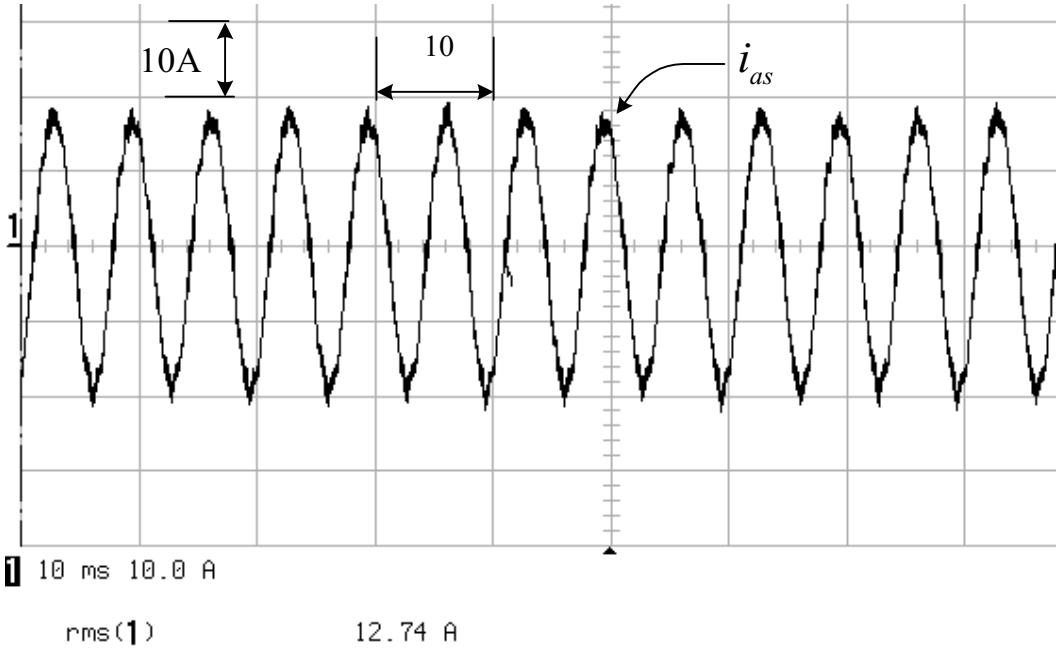

Fig. 4.13. The steady state waveform of phase-a current corresponding to Fig. 4.12.

Finally, some experiments are conducted for comparing the dynamic and steady state performances between the LTC in Chapter 2 and the proposed LMTPA control. Consider the case of applying a step command of ω_r^*=3000 rpm to the tested IPMSM drive starting from rest at t=0 sec. The corresponding steady state load torque at 3000 rpm is approximately 3.2 Nm. Fig. 4.11 shows the waveforms of the d- and q-axis current responses and speed response by using the proposed LMTPA control. From Fig. 4.11 one can see that the acceleration time period of the rotor to reach 3000 rpm is approximately 820 msec. Fig. 4.12 also records the waveforms of the phase-a current and the speed response corresponding to Fig. 4.11. The steady state waveform of phase-a current corresponding to Fig. 4.12 is also shown in Fig. 4.13. One can see that the root mean square value of the phase-a current is 12.74 A. Next, consider the same test condition as the previous one, but the proposed LMTPA control strategy is replaced by the LTC in Chapter 2 and all other parameters of speed and current controllers are kept the same as the previous one. Fig. 4.14 shows the

corresponding waveforms of the d- and q-axis current responses and speed response. In Fig. 4.14, one can see that the acceleration time period is approximately 1060 msec which is longer than that of Fig. 4.11, namely 820 msec. Fig. 4.15 also records the waveforms of the phase-a current and the speed response corresponding to Fig. 4.14. The steady state waveform of the corresponding phase-a current is also shown in Fig. 4.16. One can see that the root mean square value of the phase-a current is approximately 13.24 A which is larger than that in Fig. 4.13, namely 12.74 A. Hence, one can see that the enhancement of the dynamic speed response (i.e. the accelerating time period) by the proposed LMTPA control is about 2.3% and the reduction of the copper loss (i.e. the line current magnitude) by the proposed LMTPA control is about 3.5%.

From the above four experimental tests, one can see that the proposed LMTPA control not only can indeed achieve a linear control over the entire speed operation range but also has a larger maximum torque to enhance the dynamic performance and a smaller line current magnitude to reduce the copper loss. These experimental results indeed agree with the theoretical prediction.

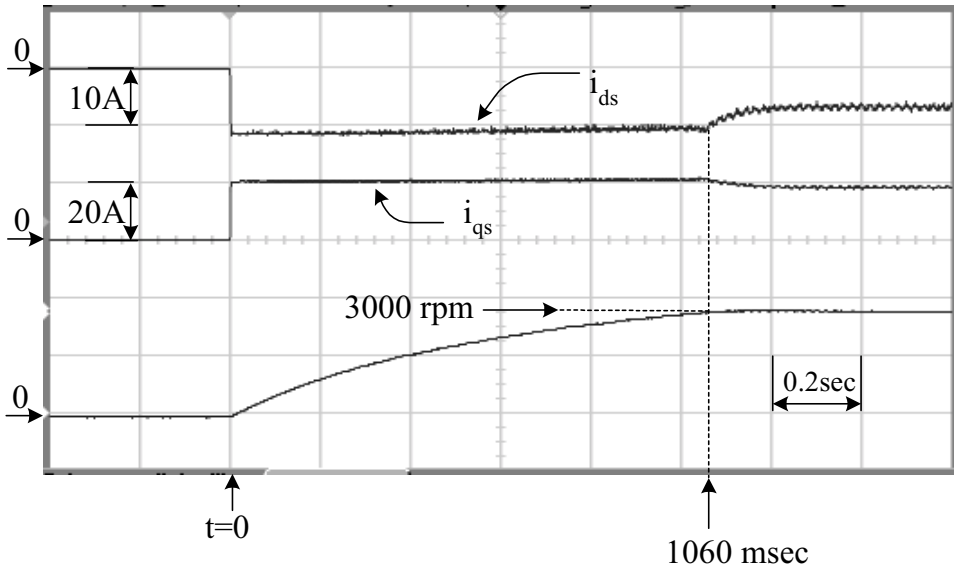

Fig. 4.14. Experimental results of i_{ds}, i_{qs}, and motor speed responses by the LTC.

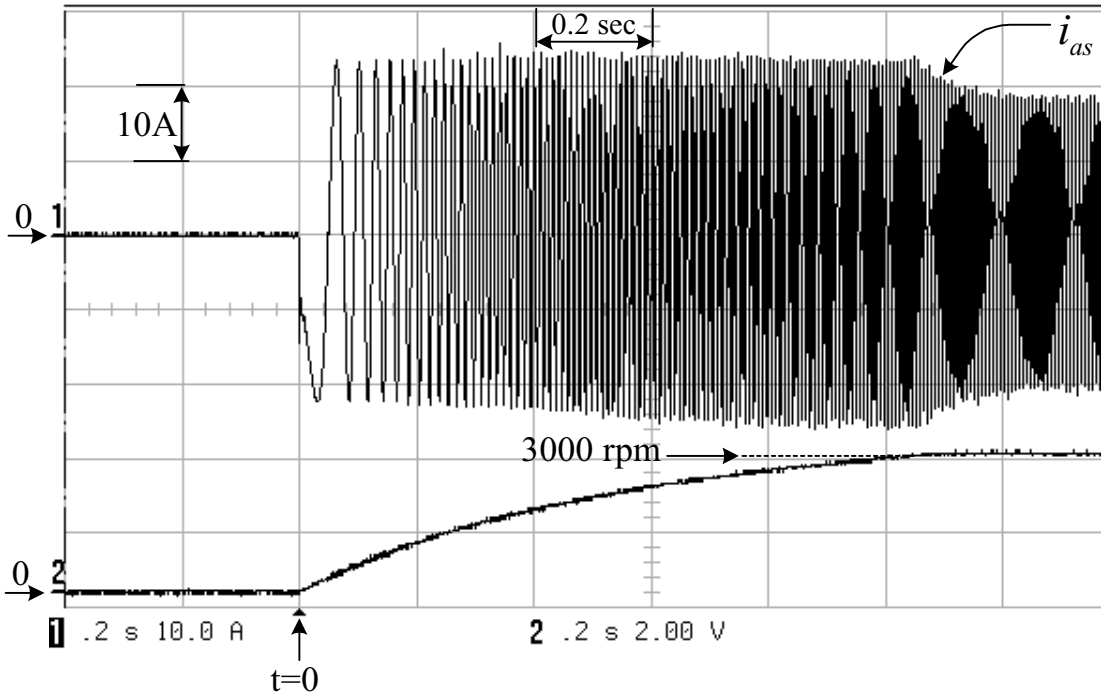

Fig. 4.15. The waveforms of the phase-a current response and the speed response corresponding to Fig. 4.14.

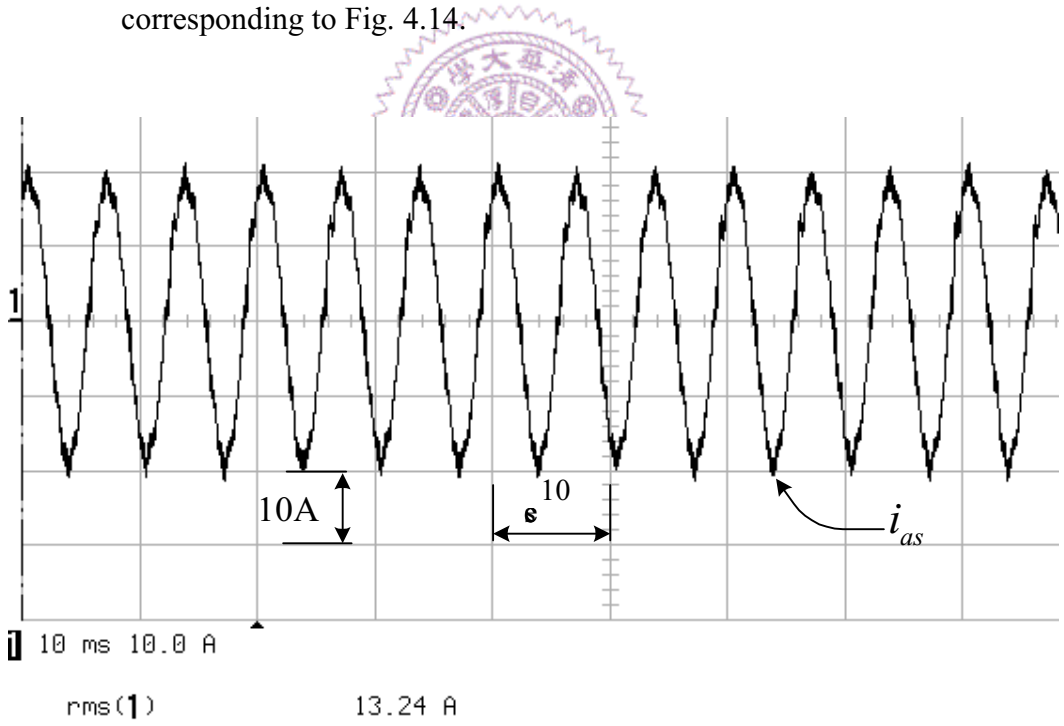

Fig. 4.16. The steady state waveform of phase-a current corresponding to Fig. 4.15.